01

# Modeling the spectral shift of the higher-frequency Q-branch of the $v_1/2v_2$ CO<sub>2</sub> Fermi dyad using spherically symmetric potentials

© A.A. Valeev

Volgograd State Technical University, Volgograd, Russia

e-mail: a\_valeev@vstu.ru

Received April 12, 2025

Revised May 19, 2025

Accepted May 19, 2025

In this work is determined the type of spherically symmetric interaction potential of molecules and its parameters to reproduce the dependences of pressure and configurational internal energy of carbon dioxide on density and temperature. Using the change in potential during vibrational excitation, a model of experimental dependences of the spectral shift of the higher-frequency Q-branch of the  $v_1/2v_2$  Fermi dyad on density is constructed.

Keywords: carbon dioxide, CARS, spectral shift, molecular dynamics, Mie potential.

DOI: 10.61011/EOS.2025.06.61660.7532-25

# Introduction

Carbon dioxide takes part in many processes on Earth and other planets. It's playing a key role in forming a planet's climate. Definitely, one can't ignore such an actual problem as global warming. On the other hand, the applied significance of this substance is also considerable. It is difficult to overestimate the role it plays in medicine and industries such as food and perfumery. Carbon dioxide in liquid and supercritical states is used for extraction [1,2] and impregnation [3]. Spontaneous Raman spectroscopy and coherent anti-Stokes Raman scattering spectroscopy (CARS) enable inexpensive and rapid analysis of thermodynamic state and chemical composition. The determination of CO<sub>2</sub> density via measurement of the frequency shifts of Q-branches of the  $v_1/2v_2$  Fermi dyad has already been achieved [4,5]. One of the key aspects of the correct operation of such devices lies in accounting for the fact that the dependence of frequency shift on density across a wide density range generally does not follow a linear relationship due to several effects. Among these is the local density augmentation effect, which manifests in the effective average density in the vicinity of a molecule being higher than the overall average density of the substance, particularly near the critical point. Local density augmentation begins occurring even at relatively low densities due to the formation of transient dimers [6], which can be considered the smallest possible clusters [7]. As the critical point is approached, cluster sizes increase.

Modeling the dependence of  $v_1/2v_2$  Fermi dyad frequencies on density using molecular dynamics methods has already been performed in [8]. In the present study, an upside-down approach will be employed: based on known dependencies [4,9] of frequency on density of  $1388 \, \mathrm{cm}^{-1}$  the higher-frequency Q-branch, the change in the effective interaction potential between two molecules upon vibrational excitation of one of them will be estimated.

To reduce the number of parameters to be determined, spherically symmetric intermolecular interaction potentials were chosen. The potential parameters must ensure agreement with experimental data (available as empirical equations) of certain macroscopic fluid characteristics.

# Determination of the potential and its parameters

The most widely recognized among spherically symmetric intermolecular potentials is the Lennard-Jones potential, depending on only two parameters:

$$u(r) = 4\varepsilon \left[ \left( \frac{\sigma}{r} \right)^{12} - \left( \frac{\sigma}{r} \right)^{6} \right].$$

A difficulty arises in that no single set of these parameters exists for CO<sub>2</sub> (see Table 1 in [10]). Parameters are typically selected to optimally suit the specific task. Since the experimental data considered in this work relate to temperatures near the critical point, parameters for the current task will be selected such that critical temperature and density match experimental values. Critical values of reduced thermodynamic quantities  $T^* = k_B T / \varepsilon$ ,  $\rho^* = \rho \sigma^3 / M$ ,  $P^* = P \sigma^3 / \varepsilon$  for a model fluid composed of particles interacting pairwise via the Lennard-Jones potential are given in [11]:  $T^* = 1.326$ ,  $\rho^* = 0.316$ ,  $P^* = 0.111$ . Here T,  $\rho$ , P,  $k_B$  are temperature, density, pressure, and the Boltzmann constant respectively,  $\varepsilon$ ,  $\sigma$  are Lennard-Jones potential parameters, and  $M = 44.010 \cdot 10^{-3} \text{ kg/mol}$  is the molar mass of carbon dioxide. From the values of critical temperature and density, both parameters are calculated as follows:  $\varepsilon = 229.3567 \,\mathrm{K} \cdot k_B$ ,  $\sigma = 0.3668915 \,\mathrm{nm}$ . For model validation, the critical pressure is obtained using  $P^* = 0.111$ , yielding:  $P = 0.111 \varepsilon / \sigma^3 = 7.12 \,\text{MPa}$ , which compares reasonably well with the experimentally established value [12]:  $P_c = 7.3773 \,\mathrm{MPa}$ . Prior to using the model, its capacity to reproduce pressure across a wide density range at 306.15 K (33 °C) was tested. than plotting pressure itself, a related quantity called semielasticity [13] of specific internal energy with respect to  $\sigma$  was computed:

$$3\left(\frac{MP}{R\rho} - T\right) = \frac{1}{k_B} \left\langle \frac{\partial u}{\partial \ln \sigma} \right\rangle,\tag{1}$$

where M is the molar mass of  $CO_2$ , R is the universal gas constant, and  $\langle u \rangle$  — denotes the average intermolecular potential energy per molecule. The calculation results within the Lennard-Jones model are shown in Figure 1, the former utilizing the equation of state from [14]. Molecular dynamics simulations were also performed. The number of molecules was set to 2048. Periodic boundary conditions were applied. Forces and potentials were truncated beyond  $5\sigma$ . Integration of mechanical equations employed a hybrid NVT/NVE scheme: initially, particle count, volume, and temperature were fixed, with temperature maintained via kinetic energy monitoring; subsequently, temperature control was disabled, allowing the system to evolve under constant energy for a certain period, at the final stage of which necessary characteristics were accumulated to compute average values. The averaging time was predominantly 3 ps, except for two density values (545 and 900 kg/m<sup>3</sup>), where it was extended to 6 and 4.2 ps respectively to minimize deviation of average temperature from 33 °C. Simulation results shown in Figure 1 exhibit significant scatter and upward deviation near the critical density. Comparing semielasticity (1) modeling results with those obtained via a high-accuracy empirical equation of state [15] (Figure 1), the model demonstrates satisfactory pressure prediction capability. Beyond pressure agreement, (configurational) internal energy must also align. Figure 2 displays plots of configuration internal energy per molecule (divided by  $k_B$ ) versus density. Included are results from the Lennard-Jones model equation of state [14] and molecular dynamics simulations. While computational and simulation results coincide well, they noticeably differ from those obtained via a reference empirical equation of state [16], also presented in Figure 2. Regrettably, tuning  $\varepsilon$  and  $\sigma$  parameters fails to simultaneously align both pressure and internal energy with the experimental values.

To eliminate this discrepancy, the Mie potential (equation (2) in [10]) was considered as a prospective candidate:

$$u(r) = \frac{\lambda_r}{\lambda_r - \lambda_a} \left(\frac{\lambda_r}{\lambda_a}\right)^{\frac{\lambda_a}{\lambda_r - \lambda_a}} \varepsilon \left[\left(\frac{\sigma}{r}\right)^{\lambda_r} - \left(\frac{\sigma}{r}\right)^{\lambda_a}\right].$$

This potential includes two additional parameters beyond  $\varepsilon$  and  $\sigma$ :  $\lambda_r$ ,  $\lambda_a$ . When they are set to 12 and 6 respectively, it reduces to the Lennard-Jones potential. [10] justifies applying this potential for carbon dioxide due to complex molecular interactions, including significant quadrupole-quadrupole contributions. Authors of [10] developed a SAFT-VR equation of state for such a fluid (Mie fluid), enabling computation of its properties through

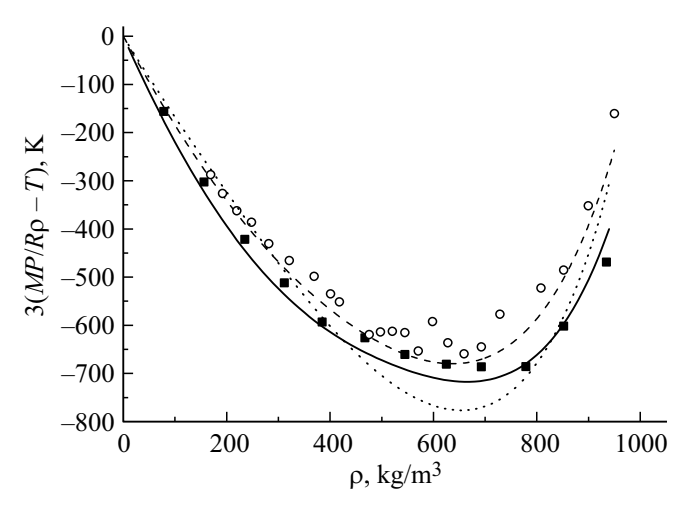
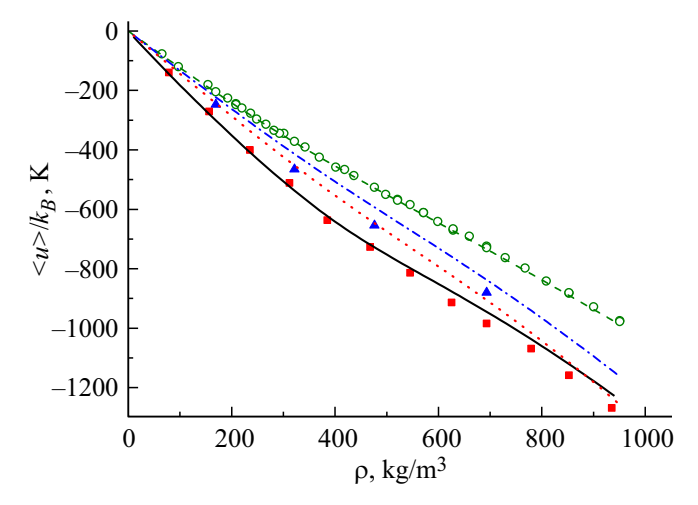


Figure 1. Dependence of internal energy semi-elasticity with respect to  $\sigma$  on density at 33 °C. Dashed and dotted lines represent calculation results using equations of state for Lennard-Jones and Mie potentials respectively. Molecular dynamics simulation results for these potentials are shown as circles and squares. The solid line indicates values obtained via the high-accuracy empirical equation of state.



**Figure 2.** Dependence of  $< u > /k_B$  on  $\rho$  at 33 °C. Dashed and dotted lines correspond to calculation results using equations of state for Lennard-Jones and Mie potentials. Molecular dynamics simulation results for these potentials are shown as circles and squares. The solid line represents values from the high-accuracy empirical equation of state. The dash-dot line and triangles show calculation results via equation of state and molecular dynamics for the Mie potential with parameters from [10].

argument values substitution into approximate equations. They also determined Mie potential parameters by fitting SAFT-VR equations to experimental data on saturated vapor pressure and coexisting liquid-phase density of CO2 over a temperature range from the triple point to  $T/T_c = 0.9$ , where  $T_c \approx 304.1 \,\mathrm{K} \,(31 \,^{\circ}\mathrm{C}) \,[12]$  is the critical temperature. This data selection differs somewhat from the 22-50 °C temperature range of our experimental dependencies, moti596 A.A. Valeev

vated by reduced SAFT-VR model accuracy near the critical point. Parameters from [10] were used with the SAFT-VR model to obtain configuration internal energy dependence on density at 33 °C (Fig. 2), showing significantly improved agreement with generalized experimental data. sponding molecular dynamics results displayed even better agreement at the same parameter values. To further improve correspondence, this work similarly approximated available through the empirical equation experimental data using the SAFT-VR model for the Mie potential. Unlike [10], the maximum temperature during phase equilibrium data fitting was set close to critical 304 K. Data from the 33 °C isotherm were also included. During this procedure, the configuration internal energy was also fitted. As a result, the following parameter values were obtained:  $\varepsilon = 434.98 \,\mathrm{K} \cdot k_B$ ,  $\sigma = 0.379272 \text{ nm}, \ \lambda_r = 20.1068, \ \lambda_a = 9.11394.$ parameters were used to compute dependencies of internal energy semi-elasticity with respect to  $\sigma$  and configuration internal energy on density via SAFT-VR equations. Results appear in Figures 1 and 2 respectively, alongside molecular dynamics simulation results with 6 ps averaging time. Noticeably, deviations from experimental data decreased. Some discrepancy remains near critical density in Figure 1, possibly arising when correlation length approaches or exceeds simulation cell dimensions. The critical temperature of the Mie-potential fluid at these parameters is 299.5 K [17], which may be considered agreeing with its experimental value in the context of the problem.

It is worth pointing out that the obtained potential parameters should be regarded as effective. They must not be used outside context, e.g., for determining long-range molecular interactions. However, they remain applicable for simulating moderately dense systems via molecular dynamics, Monte Carlo, and similar methods.

# Change in excited molecule potential

Assume the variation  $\delta u(r)$  of the interaction potential between two molecules due to vibrational excitation of one of them is small. The corresponding change in average interaction energy of such a molecule with others in the ground vibrational state becomes:

$$\Delta < u > = n \int_{0}^{\infty} F(r) \delta u(r) 4\pi r^2 dr,$$

where n is molecular concentration, F(r) is the pair correlation function, and r — is the distance between molecular centers. This energy change is responsible for the spectral frequency shift.

Since u(r) here represents the Mie potential, its first-order variation is expressed through parameter changes:

$$\delta u(r) = \frac{\partial u(r)}{\partial \varepsilon} \Delta \varepsilon + \frac{\partial u(r)}{\partial \sigma} \Delta \sigma + \frac{\partial u(r)}{\partial \lambda_r} \Delta \lambda_r + \frac{\partial u(r)}{\partial \lambda_a} \Delta \lambda_a.$$

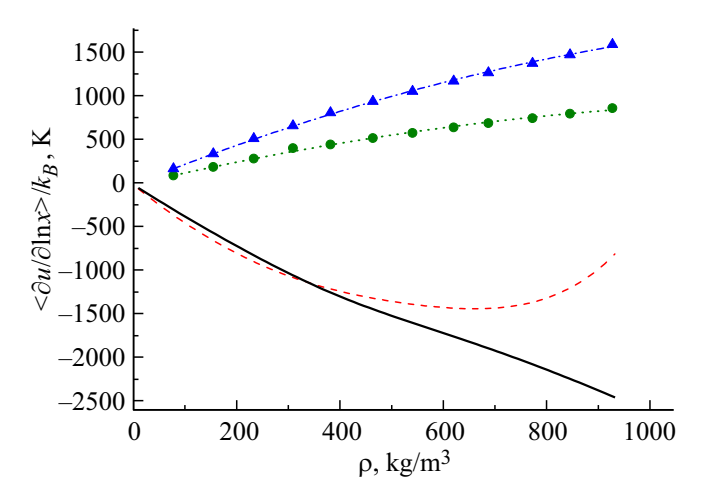


**Figure 3.** Dependencies of averaged quantities on density at 33 °C:  $< \partial u/\partial \ln \varepsilon > /k_B$  (solid line),  $< \partial u/\partial \ln \sigma > /k_B$  (dashed line),  $< \partial u/\partial \ln \lambda_r > /k_B$  (circles),  $< \partial u/\partial \ln \lambda_a > /k_B$  (triangles). Quadratic approximations of the latter two are shown with dotted and dash-dot lines.

Parameters  $\varepsilon$  and  $\sigma$  are small in SI units. Therefore, for convenience,  $\delta u(r)$  is expressed through relative parameter changes:  $\Delta \varepsilon / \varepsilon \approx \Delta \ln \varepsilon$ ,  $\Delta \sigma / \sigma \approx \Delta \ln \sigma$ ,  $\Delta \lambda_r / \lambda_r \approx \Delta \ln \lambda_r$ ,  $\Delta \lambda_a / \lambda_a \approx \Delta \ln \lambda_a$ :

$$\delta u(r) = \frac{\partial u}{\partial \ln \varepsilon} \Delta \ln \varepsilon + \frac{\partial u}{\partial \ln \sigma} \Delta \ln \sigma$$
$$+ \frac{\partial u}{\partial \ln \lambda_{\sigma}} \Delta \ln \lambda_{r} + \frac{\partial u}{\partial \ln \lambda_{\sigma}} \Delta \ln \lambda_{a}.$$

It's worth noting the first term can be replaced by  $u\Delta \ln \varepsilon$ . After averaging:

$$\Delta < u > = 2 < u > \Delta \ln \varepsilon + \left\langle \frac{\partial u}{\partial \ln \sigma} \right\rangle \Delta \ln \sigma$$
$$+ \left\langle \frac{\partial u}{\partial \ln \lambda_r} \right\rangle \Delta \ln \lambda_r + \left\langle \frac{\partial u}{\partial \ln \lambda_a} \right\rangle \Delta \ln \lambda_a.$$

The factor of 2 arises from the absence of 1/2 coefficient in  $\Delta < u >$  versus its presence in < u >:

$$\langle u \rangle = \frac{n}{2} \int_{0}^{\infty} F(r)u(r)4\pi r^{2}dr.$$

The high-accuracy empirical equation of state-derived dependence of  $<\partial u/\partial \ln \varepsilon > /k_B = 2 < u > /k_B$  on density at  $t=33\,^{\circ}\mathrm{C}$  appears in Fig. 3. The coefficient  $<\partial u/\partial \ln \sigma >$ , in the second term, as mentioned in equation (1), relates to pressure (twice the  $<\partial u/\partial \ln \sigma >$  value in that equation due to the above reason), also obtained via empirical equation. Dependence of  $<\partial u/\partial \ln \sigma > /k_B$  on density is also plotted along with other averages,  $<\partial u/\partial \ln \lambda_r > /k_B$  and  $<\partial u/\partial \ln \lambda_a > /k_B$ , found using molecular dynamics for 12 density values evenly distributed in the range corresponding to the experimental results and

ensuring the model validity. To determine these quantities at all relevant arguments, simulation results were approximated with second-order polynomials:

$$\left\langle \frac{\partial u}{\partial \ln \lambda_r} \right\rangle / k_B = 647y - 107.9y^2,$$
$$\left\langle \frac{\partial u}{\partial \ln \lambda_q} \right\rangle / k_B = 1120y - 161.2y^2.$$

From here on  $y = \rho/\rho_c$ , where  $\rho_c = 467.6 \text{ kg/m}^3$  is the critical density. Approximating polynomials are displayed as curves in Fig. 3.

To determine excited molecule parameter changes, spectroscopic dependence [9] of the  $\nu_1/2\nu_2$  Fermi dyad  $1388\,\mathrm{cm^{-1}}$  Q-branch frequency on density measured at  $33\,^{\circ}\mathrm{C}$  was approximated using  $<\Delta u/k_B>$  expansion over these functions. For improved accuracy, dependencies [4], measured at 22 and  $50\,^{\circ}\mathrm{C}$  were also utilized. The objective function becomes:

$$\begin{split} F &= \frac{1}{12} \\ &\times \sum_{i=1}^{4} \left( \frac{\nu_{i}(22\,^{\circ}\mathrm{C}) - \nu_{0}(22\,^{\circ}\mathrm{C}) - \gamma < \Delta u(22\,^{\circ}\mathrm{C}, \rho_{i})/k_{B} >}{\nu_{i}(22\,^{\circ}\mathrm{C})} \right)^{2} \\ &+ \frac{1}{18} \\ &\times \sum_{i=1}^{18} \left( \frac{\nu_{i}(33\,^{\circ}\mathrm{C}) - \nu_{0}(33\,^{\circ}\mathrm{C}) - \gamma < \Delta u(33\,^{\circ}\mathrm{C}, \rho_{i})/k_{B} >}{\nu_{i}(33\,^{\circ}\mathrm{C})} \right)^{2} \\ &+ \frac{1}{12} \\ &\times \sum_{i=1}^{12} \left( \frac{\nu_{i}(50\,^{\circ}\mathrm{C}) - \nu_{0}(50\,^{\circ}\mathrm{C}) - \gamma < \Delta u(50\,^{\circ}\mathrm{C}, \rho_{i})/k_{B} >}{\nu_{i}(50\,^{\circ}\mathrm{C})} \right)^{2}. \end{split}$$

Here  $v_i(T)$  is the measured [4,9] frequency (in cm<sup>-1</sup>) at temperature T and density  $\rho_i$ .  $<\Delta u/k_B>$  is the approximating function, also dependent on the changes in the logarithms of the parameters. The numerical factor  $\gamma=0.695034800~{\rm cm^{-1}/K}$  converts units from Kelvin to reciprocal centimeters. Additional fitting parameters are zero-density limit frequencies  $v_0$ , which depend on both temperature and experimental conditions. Note that dependencies in [4] are presented as smooth curves rather than discrete points, which made it possible in their respect to use (including molecular dynamic calculations) the same density values as have been used for the temperature 33 °C. These very densities are used in the first and third sums.

Minimization of the objective function yields relative parameter changes (table). Associated change in molecular interaction potential energy  $\Delta u(r)/k_B$  is shown in Fig. 4. The vertical line indicates the effective hard-sphere diameter of approximately 0.374 nm at considered temperatures. Values to the left of this line hold little significance due to low probability.

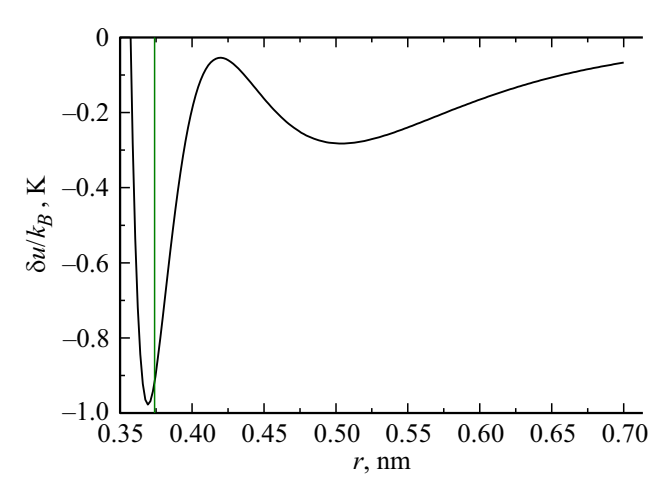


**Figure 4.** Change in the potential energy of interaction of two  $CO_2$  molecules during vibrational excitation of one of them at a frequency of  $1388 \, \text{cm}^{-1}$ .

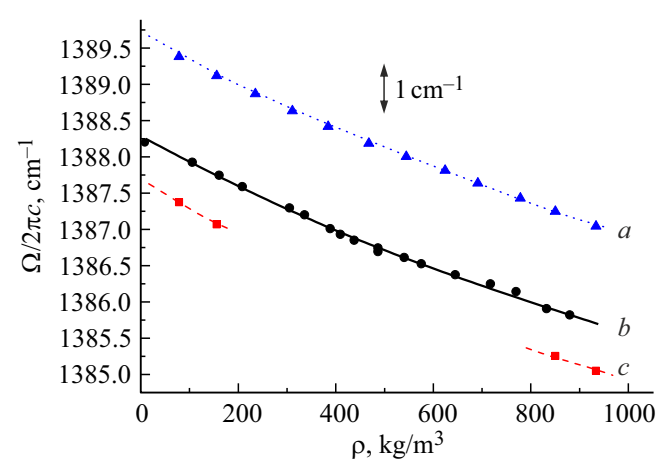


**Figure 5.** Approximated experimental dependencies on density of central frequency of  $1388 \,\mathrm{cm}^{-1}$  Q-branch of the  $v_1/2v_2$  Fermi dyad: (a) at  $50\,^{\circ}\mathrm{C}$  (measurements: dotted line, approximation: triangles), (b) at  $33\,^{\circ}\mathrm{C}$  (measurements: circles, approximation: solid line), (c) at  $22\,^{\circ}\mathrm{C}$  (measurements: dashed line, approximation: squares). Graphs (a) and (c) are shifted by +1 and  $-1\,\mathrm{cm}^{-1}$  respectively.

Fig. 5 shows approximated experimental dependences of Q-branch frequencies on density.

#### Conclusion

This work investigated modeling the density-induced frequency shift of the  $1388\,\mathrm{cm^{-1}}$  high-frequency Q-branch in  $\mathrm{CO_2}~\nu_1/2\nu_2$  Fermi dyad using particles interacting via spherically symmetric potentials. The Lennard-Jones potential proved unsuitable for this purpose failing to accurately reproduce pressure and configurational internal energy simultaneously. The Mie potential was chosen instead, with parameters determined to reproduce experimental dependencies of carbon dioxide pressure and configuration

598 A.A. Valeev

Relative Mie potent	al parameter	changes a	nd other	fitting parameters
---------------------	--------------	-----------	----------	--------------------

$\Delta arepsilon /arepsilon$	$\Delta\sigma/\sigma$	$\Delta \lambda_r/\lambda_r$	$\Delta \lambda_a/\lambda_a$	$\nu_0(22^{\circ}\mathrm{C})$	ν <sub>0</sub> (33 °C)	$\nu_0(50^{\circ}\mathrm{C})$
$(2.3 \pm 5.5) \cdot 10^{-4}$	$(-4.5 \pm 5.5) \cdot 10^{-5}$	$(2.5 \pm 4.3) \cdot 10^{-3}$	$(-3.4 \pm 2.3) \cdot 10^{-3}$	$1388.65 \\ \pm 0.04  \mathrm{cm}^{-1}$	$1388.29 \\ \pm 0.04  \mathrm{cm}^{-1}$	$1388.66 \\ \pm 0.04  \mathrm{cm}^{-1}$

internal energy on density and temperature. Then by finding appropriate relative changes in potential parameters, dependencies of the Q-branch frequencies on density were modeled. The resulting excited molecule potential change can be used for simulating other characteristics such as spectral broadening. Accuracy could be enhanced through additional experimental results.

# **Acknowledgments**

The author expresses gratitude to A.P. Kouzov for fruitful discussions and assistance.

#### Conflict of interest

The authors declare that they have no conflict of interest.

### References

- [1] E. Beckman. Science, **271** (5249), 613–614 (1996). DOI: 10.1126/science.271.5249.613
- [2] J. Kaiser. Science, 274 (5295), 2013 (1996).DOI: 10.1126/science.274.5295.2013
- V.I. Gerasimova, Yu.S. Zavorotny, A.O. Rybaltovskii, A.A. Antoshkov, V.I. Sokolov, E.V. Troitskaya, V.N. Bagratashvili. Russ. J. Phys. Chem. B, 4 (7), 1149-1157 (2010).
   DOI: 10.1134/S1990793110070158
- [4] D.M. Sublett Jr., E. Sendula, H. Lamadrid, M. Steele-MacInnis, G. Spiekermann, R.C. Burruss, R.J. Bodnar. J. Raman Spectrosc., 51, 555–568 (2020). DOI: 10.1002/jrs.5805
- [5] J. Yamamoto, Y. Hagiwara. Appl. Optics, 63 (5), 1402-1410 (2024). DOI: 10.1364/AO.507939
- [6] M.I. Cabaço, S. Longelin, Y. Danten, M. Besnard. J. Chem. Phys., 128 (7), 074507 (2008). DOI: 10.1063/1.2833493
- [7] G.A. Mel'nikov, V.N. Verveiko, Yu.F. Melikhov, M.V. Verveiko, A.V. Polyanskii. Herald of the Bauman Moscow State Technical University, Series Natural Sciences, (3), 108–123 (2011).
- [8] N.M. Asharchuk, E.I. Mareev. Russ. J. Phys. Chem. B, 18 (7), 1729–1736 (2024). DOI: 10.1134/S1990793124701021
- [9] V.G. Arakcheev, V.N. Bagratashvili, A.A. Valeev, V.B. Morozov, V.K. Popov. Russ. J. Phys. Chem. B, 4 (8), 1245–1251 (2010). DOI: 10.1134/S1990793110080117
- [10] C. Avendaño, T. Lafitte, A. Galindo, C.S. Adjiman, G. Jackson,
   E.A. Müller. J. Phys. Chem. B, 115 (38), 11154–11169 (2011). DOI: 10.1021/jp204908d
- [11] J.M. Caillol. J. Chem. Phys., 109, 4885 (1998). DOI: 10.1063/1.477099
- [12] W. Dusschek, R. Kleinrahm, W. Wagner. J. Chem. Thermodynamics, 22 (9), 841–864 (1990).
   DOI: 10.1016/0021-9614(90)90173-N

- [13] StataCorp. 2023. StataNow 18 help for margins. College Station, TX: Stata Press [Electronic source]. URL: https://www.stata.com/help.cgi?margins
- [14] J. Kolafa, I. Nezbeda. Fluid Phase Equilib., **100**, 1–34 (1994). DOI: 10.1016/0378-3812(94)80001-4
- [15] R. Span, W. Wagner. J. Phys. Chem. Ref. Data, 25 (6), 1509-1596 (1996). DOI: 10.1063/1.555991
- [16] Y. Kim. J. Mech. Sci. Technol., 21, 799-803 (2007).DOI: 10.1007/BF02916358
- N.S. Ramrattan, C. Avendaño, E.A. Müller, A. Galindo. Mol. Phys., 113 (9-10), 932-947 (2015).
   DOI: 10.1080/00268976.2015.1025112

Translated by J.Savelyeva